Electronic Supplementary Material (ESI) for Journal of Materials Chemistry A.

Supporting information

Catalytic Mechanism and Design Principle of Coordinately Unsaturated Single Metal Atom-Doped Covalent Triazine Frameworks with High Activity and Selectivity for CO_2 Electroreduction

Lele Gong[1], Xiaowei Wang[2], Tao Zheng[3], Jerry Liu[2], Jie Wang[2], Yu-Chia Yang[2], Jing Zhang[3], Xiao Han[3], Lipeng Zhang[1], Zhenhai Xia[2*]*

[1] College of Chemical Engineering, Beijing University of Chemical Technology, Beijing, 100029, China

[2] Department of Materials Science and Engineering, University of North Texas, Denton, TX 76203, USA

[3]School of Materials Science and Engineering, Northwestern Polytechnical University, Xi'an, 710072, China

* Corresponding authors: zhanglipeng2011@gmail.com, Zhenhai.xia@unt.edu

1. Free energy calculation based on CHE

The free energy of elementary reactions of CO_2 reduction is calculated based on the computational hydrogen electrode (CHE), that is, the energy of a H^+/e^- pair is equal to half of the gaseous hydrogen ($0.5H_2$) at an equilibrium potential.[1] The corrections of zero-point energy (E_{ZPE}), heat capacity (C_p), temperature (T) and entropy (S) are introduced into the DFT-calculated total energy (E_{DFT}) to determine the free energy of elementary reactions [2]:

$$G = E_{DFT} + E_{ZPE} + \int C_p d_T - TS \quad \text{(S1)}$$

where E_{ZPE}, C_p, and S are calculated from statistical mechanics within the harmonic approximation, taking the vibrational frequencies of adsorbates and molecules as calculated with DFT. It is proposed that E_{DFT} dominates in determining the free energy, while the variations in E_{ZPE}, C_p, and S corrections on different substrates are ignorable.[3] Therefore, the free energy G was calculated by using E_{DFT} plus the corrections listed in Table S3. We have calculated the corrections (E_{ZPE} + $\int C_p d_T$ - TS) for typical TM-CTFs (Table S11). The results show that the corrections vary within 8%, which are reasonable to be neglected. Therefore, the values of E_{ZPE},

C_p, and S are quoted from published reports.[4-5] Moreover, we applied an addition value of -0.51 eV into CO gaseous molecules to correct the large deviations from the standard value in using GGA-PBE functional.[6] The solvation energy correction is considered in an approximate method for COOH* intermediate by 0.25 eV and CO* intermediate by 0.1 eV since the energy differences of solvation effect for the intermediates in CO_2RR are ignorable, as shown in Table S12.[7] By applying this calculation method, the calculated equilibriums potential *vs* CHE for overall half reaction of CO_2 conversion agrees well with the experimental value *vs.* RHE (Table S2).[8]

2. Adsorption energy and overpotential calculation of TM-CTFs

To predict electrocatalytic behavior, the first elementary reaction of gaseous reactant adsorption on catalysts is considered to be one of critical steps to determine the catalytic mechanism and catalytic activity. There are four elementary reactions in CO_2RR, including CO_2 chemisorption, CO_2 activation, chemicals formation, and products desorption, as shown in Figure S1. The overall reactions of CO_2 reduction are[9]:

$$* + CO_{2(g)} \rightarrow *CO_2 \quad \text{(S2)}$$

$$*CO_2 + H^+ + e^- \rightarrow *COOH \quad \text{(S3)}$$

$$*COOH + H^+ + e^- \rightarrow *CO + H_2O_{(l)} \quad \text{(S4)}$$

$$*CO \rightarrow * + CO_{(g)} \quad \text{(S5)}$$

where * refers to the active site on the surface of catalysts, subscripts *g* and *l* stand for the gas and liquid phases, respectively. The $*CO_2$, *COOH and *CO refer to the intermediates adsorbed on TM-CTFs.

The adsorption energies are calculated with following equations.[10]

$$\Delta G_{*CO2} = G(*CO_2) - G(*) - G_{CO2} \quad \text{(S6)}$$

$$\Delta G_{COOH} = G(*COOH) - G(*) - (G_{CO2} + 0.5G_{H2}) \quad \text{(S7)}$$

$$\Delta G_{*CO} = G(*CO) - G(*) - (G_{CO2} + G_{H2} - G_{H2O}) \quad \text{(S8)}$$

where G(*) is the ground state energy of cleanly unabsorbed surface, $G(*CO_2)$, G(*COOH) and G(*CO) are the ground state energies of surface absorbed with $*CO_2$, *COOH, and *CO adsorbates on TM-CTFs, G_{CO2}, G_{H2} and G_{H2O}, are the energies of CO_2, H_2 and H_2O gaseous/liquid molecules, respectively.

The overpotential (η^{CO}) calculations is defined as:

$$\eta^{CO} = max[\Delta G_{elem}/ne] \tag{S9}$$

where n is the number of electronic transfers for each elementary reaction, and ΔG_{elem} is the free energy (ΔG_1, ΔG_2, ΔG_3, and ΔG_4) of elementary reactions (Equations S2–S5). Note here, ΔG_{elem} is calculated at equilibrium state, i.e., the free energy of the electrochemical step (ΔG_2, ΔG_3) of CO_2RR will be added -0.12V for CO product (Figure S2).

3. Kinetic calculation of TM-CTFs

In this study, we also calculated the energy barrier for producing CO or HCOOH via *COOH intermediate to determine the prioritization during second hydrogenation. The Climbing Image-Nudged Elastic Band (CI-NEB) method was utilized to calculate transition stats (TS) on TM-CTFs.[11] Five images are inserted between initial structure (IS) and final structure (FS) in our calculations. A linearized Poisson–Boltzmann implicit solvation model was used to neutralize the nonzero charge in the simulation, as implemented in VASPsol.[12] The dielectric constant is set up to 80 for water environment in simulating. The solvated proton is modelled by $H_7O_3^+$ near the reaction intermediates. The VDW method is controlled via zero damping DFT-D3 method.[13]

4. Formation energy and dissolution potential of TM-CTFs

The formation energy refers to the difficulty of synthesizing a catalyst from CTF substrate, namely thermodynamical stability. The dissolution potential represents electrochemical stability, meaning whether the metal active center will fall off the structure and dissolve into the electrolyte. An excellent catalyst should have both high thermodynamical and electrochemical stabilities. The formation energy and dissolution energy of TM-CTFs are defined as[14]:

$$E_f = E_{TM-CTF} - E_{CTF} - E_{TM} \tag{10}$$

$$U_{diss} = U^o_{diss}(metal, bulk) - E_f/ne \tag{11}$$

where E_{TM-CTF}, E_{CTF}, $and\ E_{TM}$ are the total energies of TM-CTF, substrate and metal atom, $U^o_{diss}(metal, bulk)$ and n are the standard dissolution potential of bulk metal and the number of electrons involved in the dissolution, respectively.[15] The corresponding values are shown in

Table S5.

5. The descriptor (Φ) calculation

We here proposed a rational and reliable principle for guiding the design of high activity catalysts for CO_2RR. The novel descriptor for TM-CTFs is defined as:

$$\Phi = \frac{N}{r_{TM} * n} \quad (12)$$

where N, r_{TM} and n are the number of d electrons, the atomic radius, and the periodic number of TMs, respectively, and the corresponding values are shown in Table S4. Actually, the number of d electrons (N) plays a critical role in indirectly determining the catalytic behavior. The atomic radius (r_{TM}) and periodic number (n) strongly influence the geometric configuration and topological structure in adsorbing intermediates. The CO_2RR catalytic activities , as well as its catalytic mechanism, of TM-CTFs could be predicted by utilizing this descriptor.

6. The molecule orbital of CO_2 gaseous

The molecule orbital of CO_2 was carried out using the Gaussian 09.D01 program suite.[16] The ground state geometry was optimized by the density functional theory (DFT) B3LYP (Becke's three-parameter hybrid function with the non-local correlation of Lee–Yang–Parr) method combining with the 6-31G(d) basis set.[17] Frequency analysis was performed under the same theoretical level to ensure that the structure was the local minimum on the potential energy surface. The results are shown in Figure S3.

Supplementary Tables

Table S1. The values of U-J parameters for DFT calculations.[18-22]

3d	Sc	Ti	V	Cr	Mn	Fe	Co	Ni	Cu	Zn
U-J	2.11	2.58	2.72	2.79	3.06	3.29	3.42	3.40	3.87	4.12
4d	Y	Zr	Nb	Mo	/	Ru	Rh	Pd	Ag	/
U-J	2.00	2.00	2.04	2.18	/	2.42	2.80	3.35	3.50	/
5d	/	Hf	Ta	W	Re	Os	Ir	Pt	Au	/
U-J	/	1.95	2.05	2.20	2.26	2.19	2.34	2.41	3.00	/

Table 2. The equilibrium potential (V) and calculation values (V) of reaction potential at 0 V applied voltage for CO_2RR.[8]

Half-reaction	Calculated	Equilibrium
$CO_2 + 2(H^+ + e^-) \rightarrow CO_{(g)} + H_2O_{(l)}$	-0.120	-0.12
$CO_2 + 2(H^+ + e^-) \rightarrow HCOOH_{(l)}$	-0.201	-0.20
$CO_2 + 4(H^+ + e^-) \rightarrow HCHO_{(l)} + H_2O_{(l)}$	-0.073	-0.07
$CO_2 + 6(H^+ + e^-) \rightarrow CH_3OH_{(l)} + H_2O_{(l)}$	0.031	0.03
$CO_2 + 8(H^+ + e^-) \rightarrow CH_{4\,(g)} + 2H_2O_{(l)}$	0.167	0.17
$2H^+ + 2e^- \rightarrow H_{2(g)}$	0.000	0.00

Table 3. Corrections including zero-point energy (*ZPE*), heat capacity (C_p) and entropy (*S*) at 298K for converting the calculated total energy to free energy (eV)

Adsorbate	*ZPE*	*TS*	$\int C_p dT$
$*CO_2$	0.30	0.09	0.06
*COOH	0.63	0.17	0.09
*OCHO	0.62	0.20	0.10
*HCOOH	0.82	0.09	0.05
*CO	0.22	0.08	0.05
*OH	0.40	0.04	0.03
CO_2	0.31	0.65	0.10
CO	0.14	0.67	0.09
HCOOH	0.90	1.02	0.11
H_2O	0.58	0.65	0.10
H_2	0.27	0.42	0.09

Table 4. The number of *d* electrons (N_{TM}), atomic radius (r_{TM}), and periodic number (n) of transition metals, and their corresponding descriptor (Φ).[23]

	N_{TM}	r_{TM}/Å	n	Φ
Ti	2	1.76	3	0.38
V	3	1.71	3	0.58
Cr	5	1.66	3	1.00
Mn	5	1.61	3	1.04
Fe	6	1.56	3	1.28
Co	7	1.52	3	1.54
Ni	8	1.49	3	1.79
Cu	10	1.45	3	2.30
Zn	10	1.42	3	2.35
Nb	4	1.98	4	0.51
Mo	5	1.90	4	0.66
Ru	7	1.78	4	0.98
Rh	8	1.73	4	1.16
Pd	10	1.69	4	1.48
Ag	10	1.65	4	1.52
Ta	3	2.00	5	0.30
W	4	1.93	5	0.41
Re	5	1.88	5	0.53
Os	6	1.85	5	0.65
Ir	7	1.80	5	0.78
Pt	9	1.77	5	1.02
Au	10	1.74	5	1.15

Table 5. The number of transferred electrons (N_e), standard dissolution potential (U^{o}_{diss}), the calculated formation energy (E_f) and dissolution potential (U_{diss}) of TM-CTFs.

	N_e	U^{o}_{diss}	E_f	U_{diss}
Sc	3	-2.08	-3.67	-0.86
Ti	2	-1.63	-3.45	0.09
V	2	-1.18	-2.72	0.18
Cr	2	-0.91	-2.91	0.55
Mn	2	-1.19	-1.43	1.90
Fe	2	-0.45	-1.82	0.46
Co	2	-0.28	-2.06	0.75
Ni	2	-0.26	-1.99	0.74
Cu	2	0.34	-1.03	0.86
Zn	2	-0.76	-1.74	0.11
Y	3	-2.37	-3.89	-1.07
Zr	4	-1.45	-4.36	-0.36
Nb	3	-1.10	-3.34	0.01
Mo	3	-0.20	-4.79	1.40
Ru	2	0.46	-2.21	1.57
Rh	2	0.60	-1.80	1.50
Pd	2	0.95	-2.00	1.95
Ag	1	0.80	-1.79	2.59
Hf	4	-1.55	-4.41	-0.45
Ta	3	-0.60	-3.82	0.67
W	3	0.10	-2.39	0.90
Re	3	0.30	-1.12	0.67
Os	8	0.84	-2.13	1.11
Ir	3	1.16	-2.84	2.11
Pt	2	1.18	-1.49	1.92
Au	3	1.50	-1.40	1.97

Table 6. The ICOHP values of TM-C, TM-O′ and their average in TM-CTFs-*CO_2 configuration, and the ICOHP value of C-O′ and C-O″ in *CO_2 adsorbate.

	$ICOHP^{TM-C}$	$ICOHP^{TM-O'}$	$Average$	$ICOHP^{C-O'}$	$ICOHP^{C-O''}$
Ti	-1.61	-2.93	-2.27	-3.45	-5.53
V	-1.23	-1.59	-1.41	-4.48	-7.42
Cr	-1.39	-1.62	-1.51	-4.44	-6.77
Mn	-1.10	-1.46	-1.28	-7.33	-8.57
Fe	-1.72	-1.57	-1.65	-7.07	-8.26
Co	-1.62	-1.31	-1.47	-7.58	-8.38
Ni	-1.12	-1.10	-1.11	-8.10	-8.75
Cu	-1.45	-0.65	-1.05	-7.18	-7.71
Zn	-1.48	0.00	-1.48	-7.80	-7.80
Nb	-2.12	-2.22	-2.17	-2.82	-5.32
Mo	-1.91	-1.33	-1.62	-6.64	-8.20
Ru	-1.90	-0.86	-1.38	-7.09	-8.11
Rh	-1.54	-0.66	-1.10	-7.55	-8.37
Pd	-1.73	-0.68	-1.21	-6.98	-7.68
Ag	-1.16	0.00	-1.16	-7.32	-7.36
Ta	-2.39	-2.53	-2.46	-2.69	-5.41
W	-2.05	-1.78	-1.92	-3.82	-6.16
Re	-2.00	-1.77	-1.89	-4.46	-6.28
Os	-2.15	-1.31	-1.73	-7.11	-8.37
Ir	-1.85	-0.83	-1.34	-7.13	-8.23
Pt	-1.45	0.00	-1.45	-6.92	-7.15
Au	-1.50	0.00	-1.50	-7.12	-7.36

Table 7. The overpotential of CO (η^{CO}/V), HCOOH (η^{HCOOH}/V), H_2 (η^{H2}/V) in electrocatalytic CO_2RR and HER, respectively.

	η^{CO}	η^{HCOOH}	η^{H2}
Ti	1.32	1.35	0.28
V	0.61	1.07	0.05
Cr	0.45	1.30	0.25
Mn	0.54	1.73	0.63
Fe	0.51	1.34	0.70
Co	0.42	1.38	0.77
Ni	0.34	1.66	0.46
Cu	0.51	0.76	0.32
Zn	0.86	0.97	0.81
Nb	0.91	1.03	0.31
Mo	0.55	1.18	0.13
Ru	1.12	0.57	0.41
Rh	0.81	0.54	0.13
Pd	0.56	0.72	0.25
Ag	0.50	0.77	0.63
Ta	1.67	1.21	0.64
W	1.03	1.50	0.59
Re	1.62	1.92	0.65
Os	0.77	1.08	0.63
Ir	1.46	0.43	0.47
Pt	1.30	0.49	0.77
Au	0.54	0.71	0.86

Table S8. Free energy (eV) and overpotential (η/V) of CO_2RR (η^{CO}) on noble metals.

	ΔG_1	ΔG_2	ΔG_3	ΔG_4	η^{CO}
Ag (2 1 1)	-0.02	0.98	-0.24	-0.48	0.86
Au (2 1 1)	-0.08	0.82	-0.31	-0.19	0.70

Table S9. The bond length of simulation TM-CTFs versus experimental results[24].

	TM-N_1	TM-N_2	TM-N_3	Average	Experimental
Co-CTF	2.17	1.90	2.18	2.08	2.00 ± 0.10
Ni-CTF	2.20	1.88	2.27	2.11	2.08 ± 0.05

Table S10. Representative SACs with coordinately-unsaturated transition metal for electrocatalytic CO_2RR, including Faraday efficiency (FE^{CO}/%), current density (j^{CO}/ mA cm^{-2}), and Tafel plot.

Catalysts	active site	Electrolyte	FE^{CO}	j^{CO}	Tafel	Ref
Co-CTF	$Co\text{-}N_3$	0.1 M $KHCO_3$	~ 85	-1.20 @ -1.10 V	162	24
Ni-CTF	$Ni\text{-}N_3$	0.1 M $KHCO_3$	~ 96	-1.50 @ -1.10 V	154	24
Cu-CTF	$Cu\text{-}N_3$	0.1 M $KHCO_3$	~ 12	-0.05 @ -1.10 V	305	24
Co-SAC	$Co\text{-}N_3$	0.5 M $KHCO_3$	~ 63	-18.1 @ -0.63 V	-	25
	$Co\text{-}N_2$	0.5 M $KHCO_3$	~ 91	-32.7 @ -0.78 V	-	25
C-Zn_1Ni_4 ZIF-8	$Ni\text{-}N_3$	0.5 M $KHCO_3$	~ 98	-71.5 @ -1.05 V	-	26
Cu-N_2/GN	$Cu\text{-}N_2$	0.1 M $KHCO_3$	81	-10.0 @ -0.75 V	245	27
Ni-N_3-V SAC	$Ni\text{-}N_3$	0.5 M $KHCO_3$	90	-65.0 @ -0.90 V	124	28
Fe_1NC/S_1-1000	$Fe\text{-}N_3$	0.5 M $KHCO_3$	96	-6.8 @ -0.60 V	96.5	29
Ni-N-Gr	$Ni\text{-}N_x$ (x = 2, 3)	0.1 M $KHCO_3$	~ 95	-4.0 @ -1.20 V	126	30
Ni@NCH-800	$Ni\text{-}N_2$	0.1 M $KHCO_3$	~ 86	-35.0 @ -1.00 V	-	31

Table S11. The comparison of zero-point energy (ZPE), heat capacity (C_p) and entropy (S) at 298K for Ti-CTF, Ni-CTF, Cu-CTF, and Zn-CTFs, calculated from DFT and cited from literatures

	Adsorbate	E_{ZPE}	TS	$\int C_p dT$	$E_{ZPE} + \int C_p d_T - TS$
Corrections cited [4,5]	$*CO_2$	0.30	0.09	0.06	0.27
	*COOH	0.63	0.17	0.09	0.55
	*CO	0.22	0.08	0.05	0.19
Ti-CTF	$*CO_2$	0.30	0.08	0.03	0.25
	*COOH	0.57	0.16	0.12	0.53
	*CO	0.19	0.09	0.08	0.18
Ni-CTF	$*CO_2$	0.31	0.11	0.07	0.27
	*COOH	0.63	0.17	0.08	0.54
	*CO	0.21	0.07	0.05	0.19
Cu-CTF	$*CO_2$	0.30	0.11	0.07	0.26
	*COOH	0.61	0.16	0.09	0.54
	*CO	0.20	0.08	0.08	0.20
Zn-CTF	$*CO_2$	0.29	0.10	0.06	0.25
	*COOH	0.63	0.19	0.09	0.53
	*CO	0.19	0.11	0.09	0.17

Table S12. The solvation corrections cited from previous and calculated by using the implicit solvation model for Ti-CTF, Ni-CTF, Cu-CTF, and Zn-CTFs.

	$*CO_2$	*COOH	*CO
Cited [7]	0.25	0.25	0.10
Ti-CTF	-0.41	-0.36	-0.26
Ni-CTF	0.27	0.28	0.12
Cu-CTF	0.30	0.27	0.08
Zn-CTF	0.27	0.27	0.11

Supplementary Figures

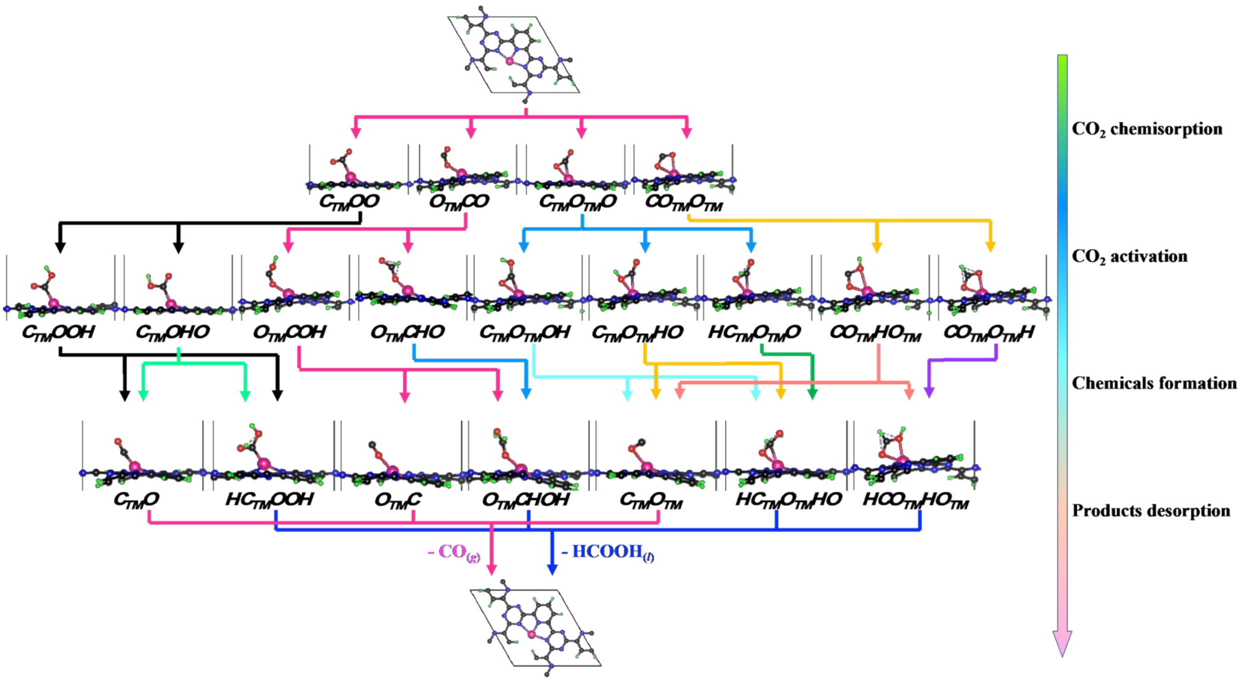

Figure S1. The possible intermediates in CO_2RR on TM-CTFs via four elementary steps, including CO_2 chemisorption, CO_2 activation, chemical formation, and product desorption, the proton and electron (H^++e^-) in the elementary reactions are omitted for simplification. The *g* and *l* represent the gas and the liquid, respectively. The black, green, blue, red and pink represent carbon, hydrogen, nitrogen, oxygen, and TM atoms, respectively.

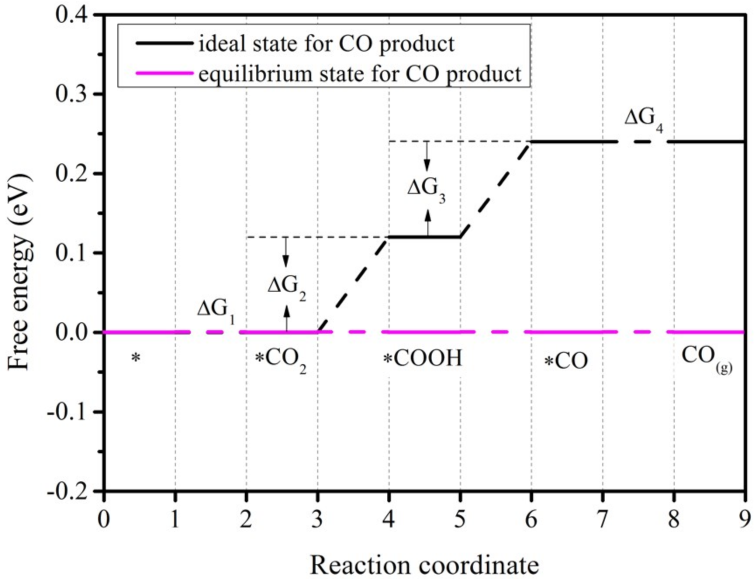

Figure S2. Free energy diagram of ideal and equilibrium states for CO_2RR toward CO on ideal electrocatalysts.

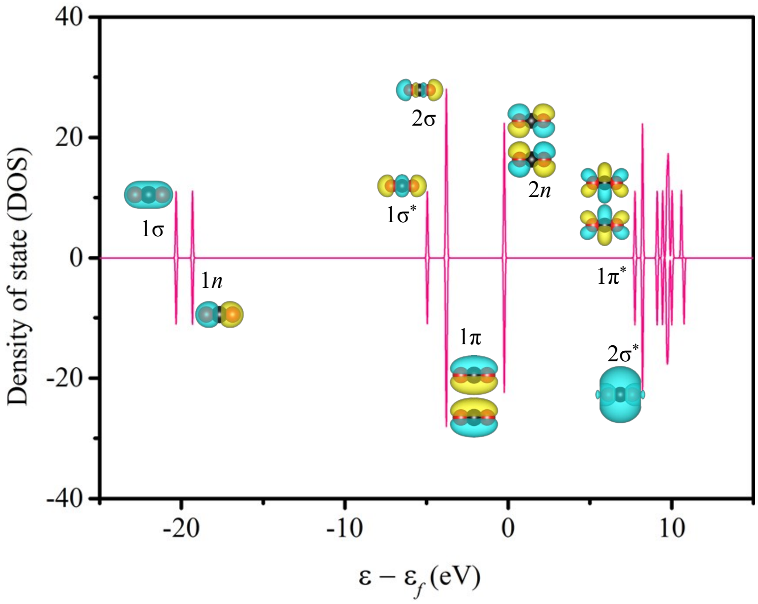

Figure S3. The molecule orbitals of free CO_2.

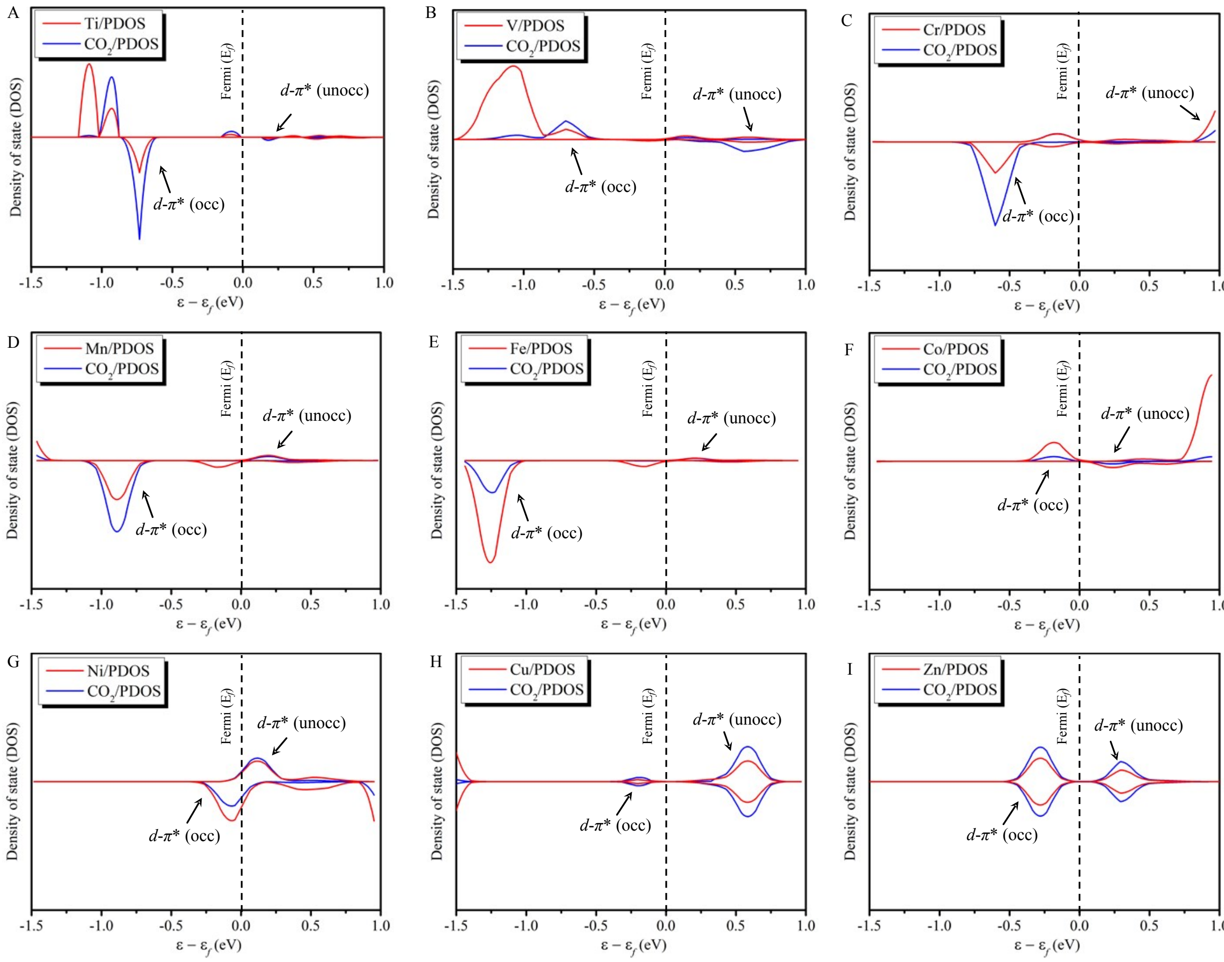

Figure S4. The DOS and PDOS calculations of typical 3d TM-CTF after adsorbing a $*CO_2$ intermediate, (A) Ti-CTF, (B) V-CTF, (C) Cr-CTF, (D) Mn-CTF, (E) Fe-CTF, (F) Co-CTF, (G) Ni-CTF, (H) Cu-CTF, (I) Zn-CTF.

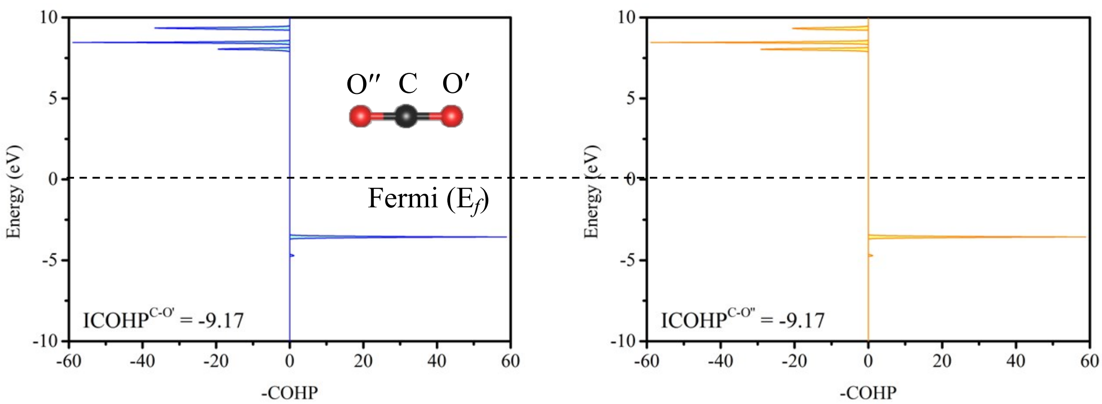

Figure S5. The COHP and ICOHP calculations of free CO_2 molecules.

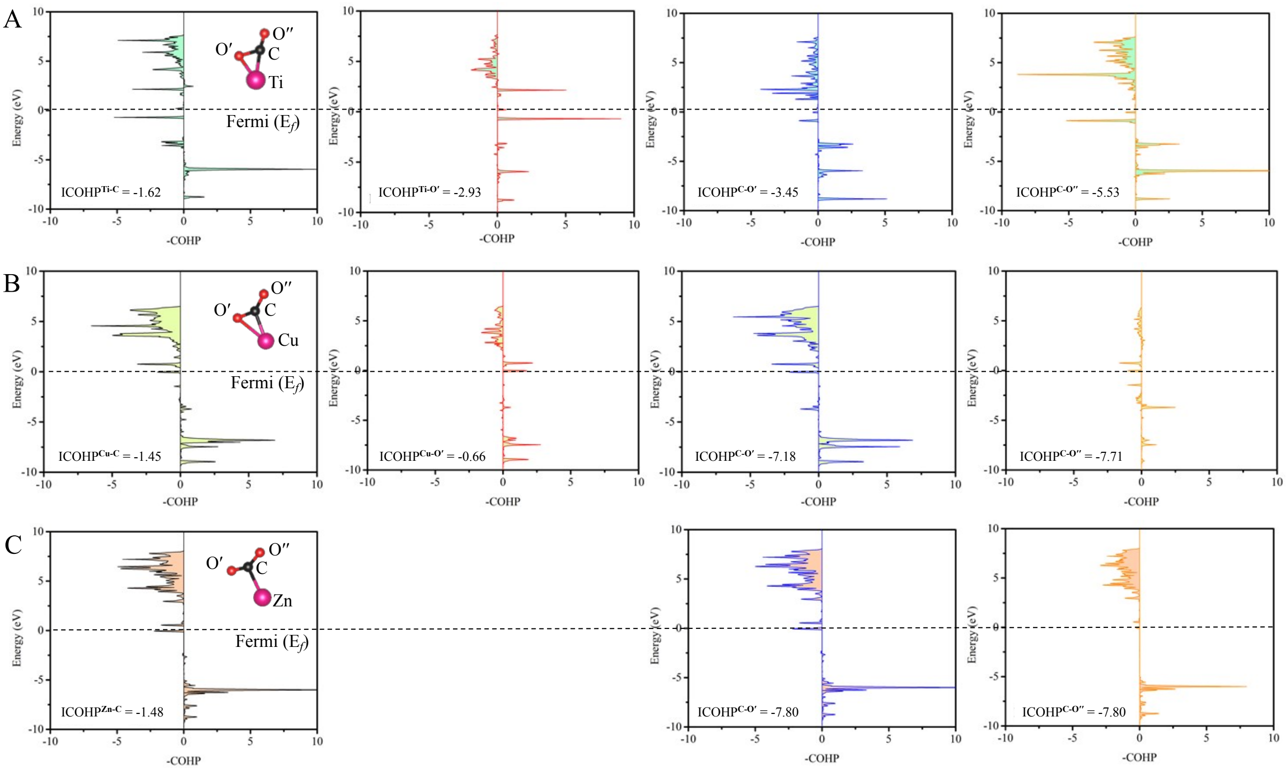

Figure S6. The COHP calculations and corresponding ICOHP values of typical TM-CTFs, A) Ti-CTF, B) Cu-CTF, C) Zn-CTF. From left to right including TM-C, TM-O′, C-O′, C-O″, respectively. The inset configuration of TM-CTF-*CO_2 was simplified for clarity.

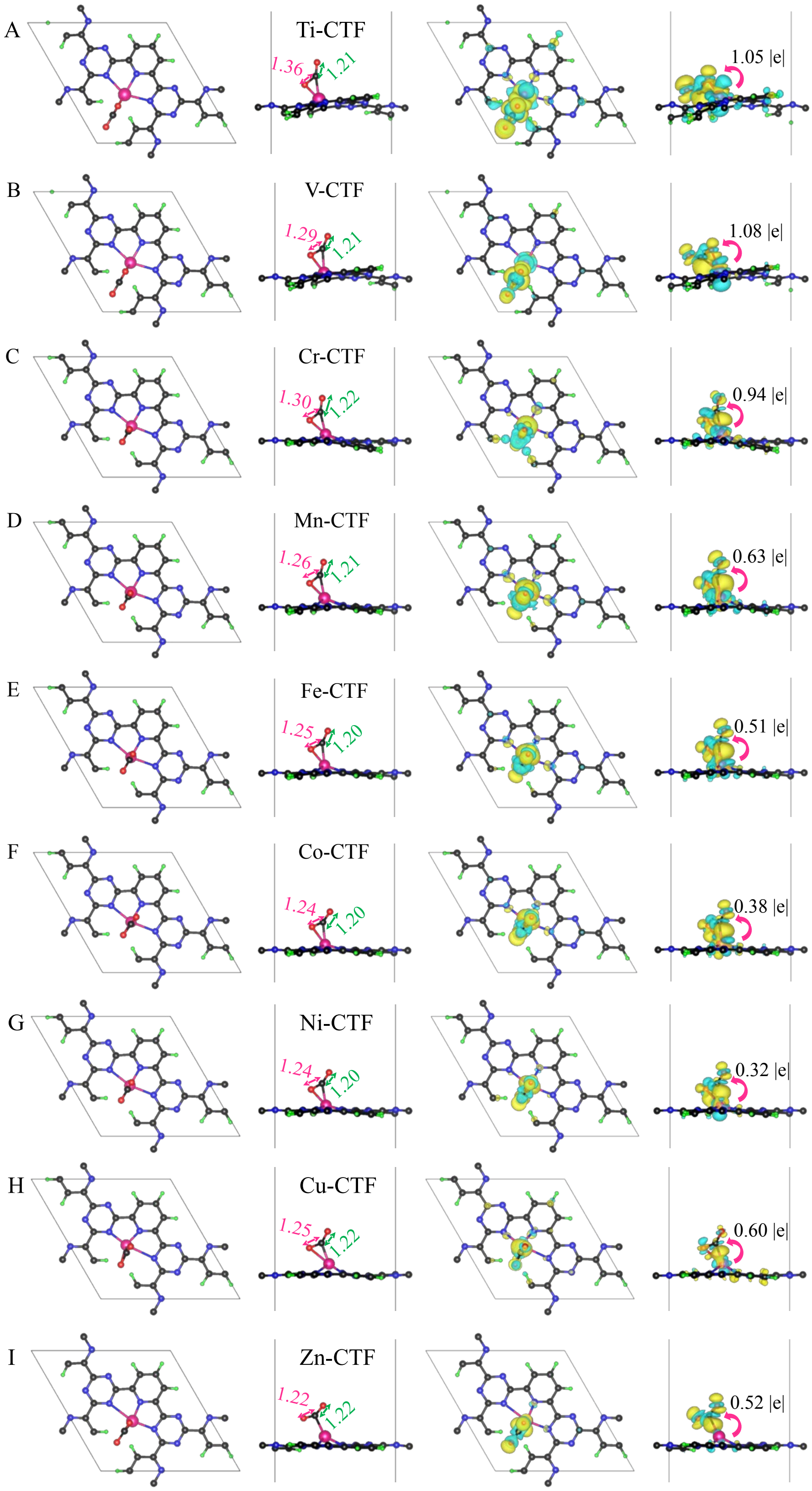

Figure S7. Optimized adsorption configurations and charge density distribution of CO_2 chemisorbed on 3*d* TM-CTF. A) Ti-CTF, B) V-CTF, C) Cr-CTF, D) Mn-CTF, E) Fe-CTF, F) Co-CTF, G) Ni-CTF, H) Cu-CTF, and I) Zn-CTF.

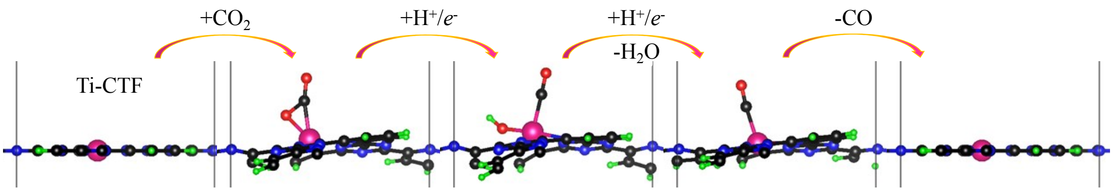

Figure S8. The elementary reactions of Path 1 on Ti-CTF. The black, green, blue, red and pink represent carbon, hydrogen, nitrogen, oxygen, and Ti atoms, respectively.

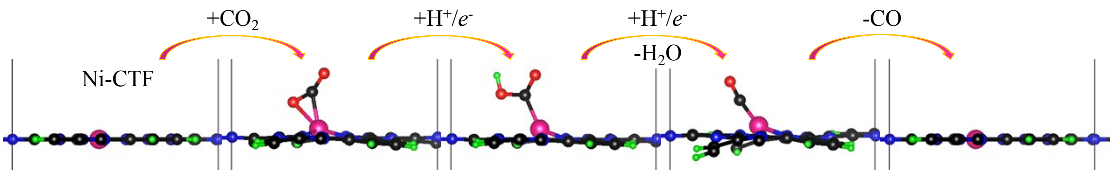

Figure S9. The elementary reaction of Path 2 on Ni-CTF. The black, green, blue, red and pink represent carbon, hydrogen, nitrogen, oxygen, and Ni atoms, respectively.

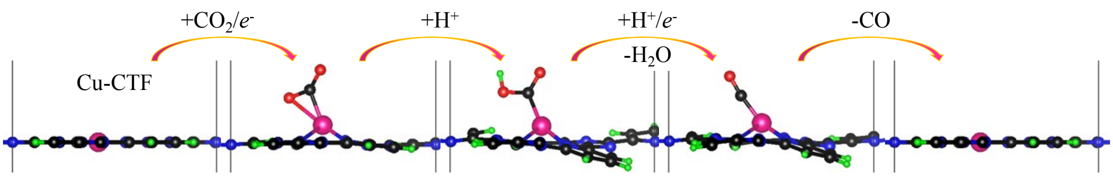

Figure S10. The elementary reaction of Path 3 on Cu-CTF. The black, green, blue, red and pink represent carbon, hydrogen, nitrogen, oxygen, and Cu atoms, respectively.

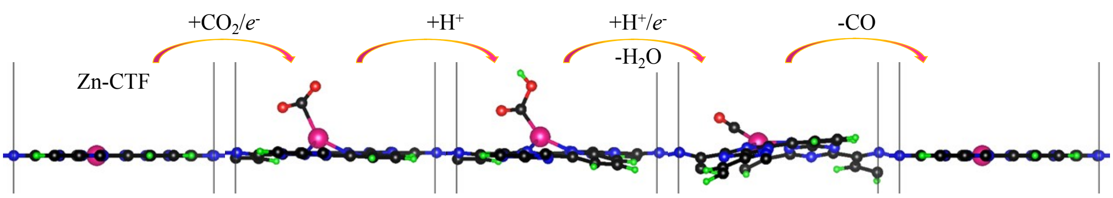

Figure S11. The elementary reaction of Path 4 on Zn-CTF. The black, green, blue, red and pink represent carbon, hydrogen, nitrogen, oxygen, and Zn atoms, respectively.

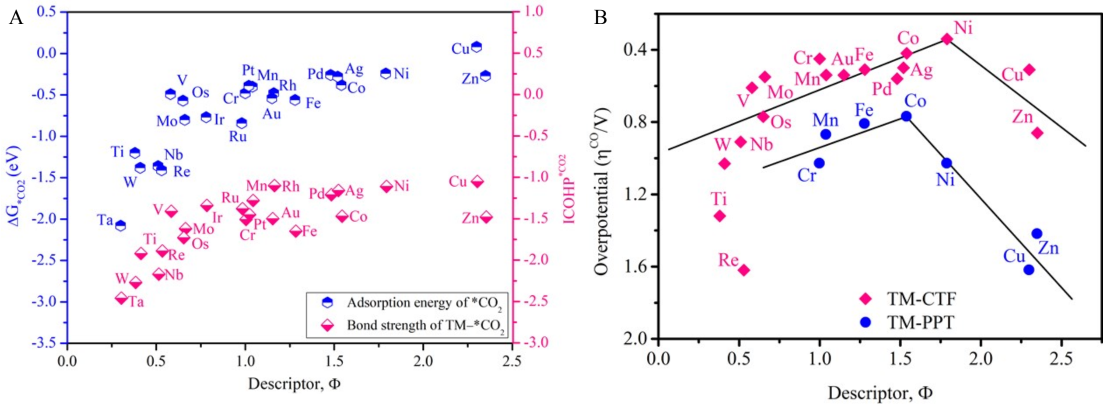

Figure S12. (A) The adsorption energy and ICOHP of CO_2 on different catalysts as a function of the descriptor. There are positive correlations between the descriptor and adsorption energy of intermediates or the bond strength of TM-intermediates; (B) A volcano-shaped relationship between the overpotential (η^{CO}) and descriptor (Φ) for TM-CTFs and TM-TPPs.

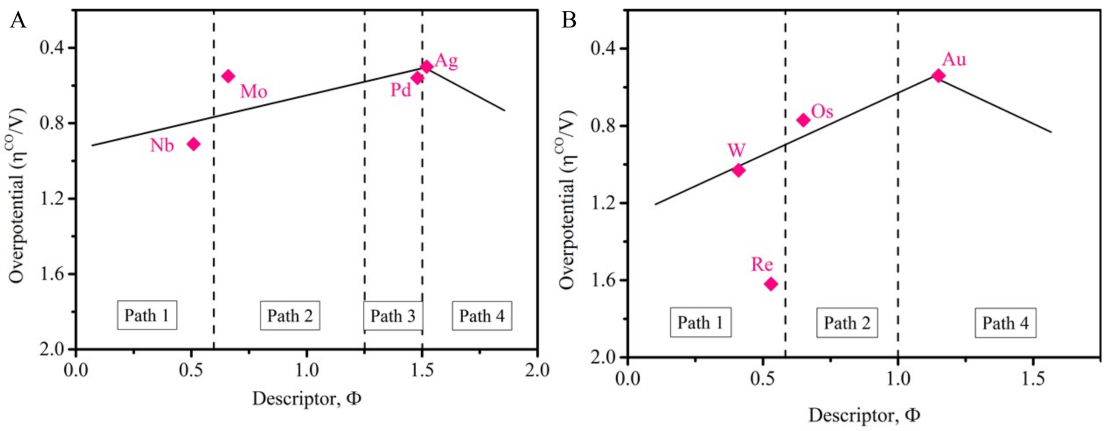

Figure S13. Volcano-shaped relationships between the overpotential (η^{CO}) and descriptor (Φ) for (A) 4d and (B) 5d TM-CTFs. Both the CO_2RR catalytic activity and mechanism are predicted by using this descriptor.

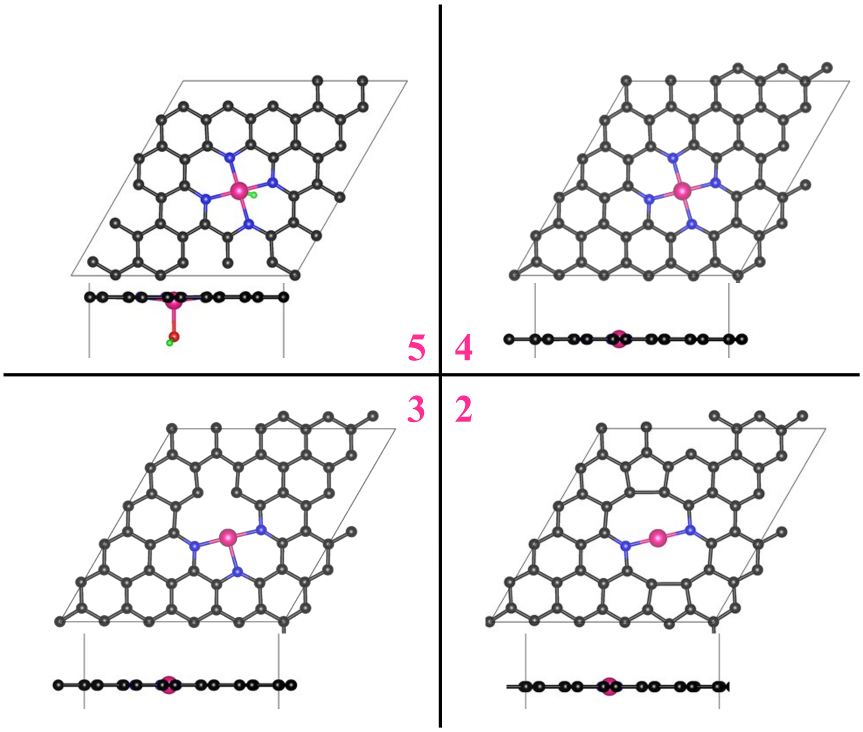

Figure S14. The geometric structures of NiN_x based catalysts with different coordinate number (x = 2 to 5) anchored on graphene substrates. The black, green, blue, red and pink represent carbon, hydrogen, nitrogen, oxygen, and Ni atoms, respectively.

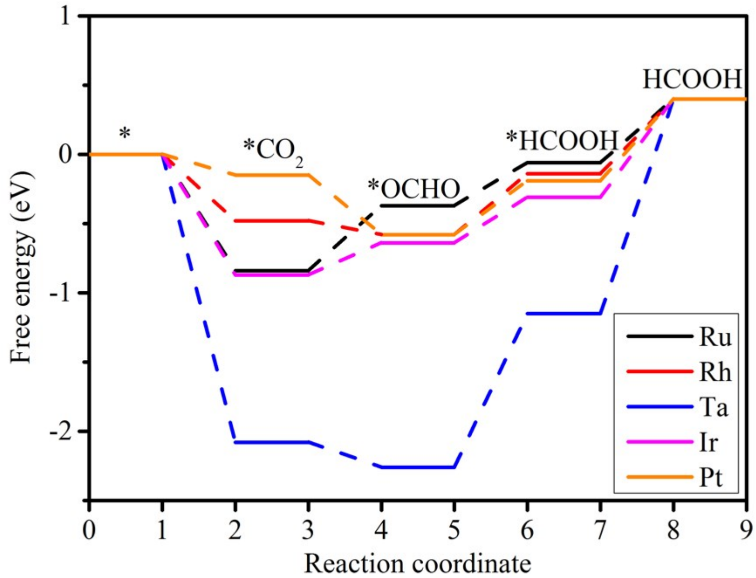

Figure S15. The free energy diagram of five TM-CTFs (Ru-CTF, Rh-CTF, Ta-CTF, Ir-CTF, Pt-CTF) in electroreduction CO_2 to HCOOH.

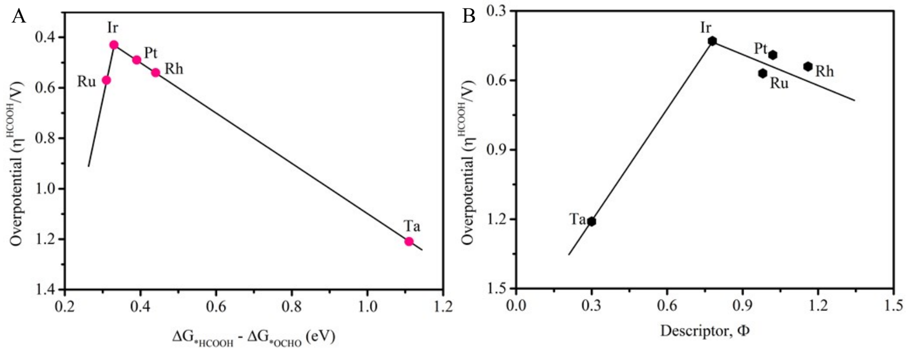

Figure S16. (A) Volcano-shaped relationship between the overpotential (η^{HCOOH}) and the adsorption energy of $\Delta G_{*HCOOH} - \Delta G_{*OCHO}$ for TM-CTFs. (B) The volcano relationship between the overpotential (η^{HCOOH}) and descriptor (Φ).

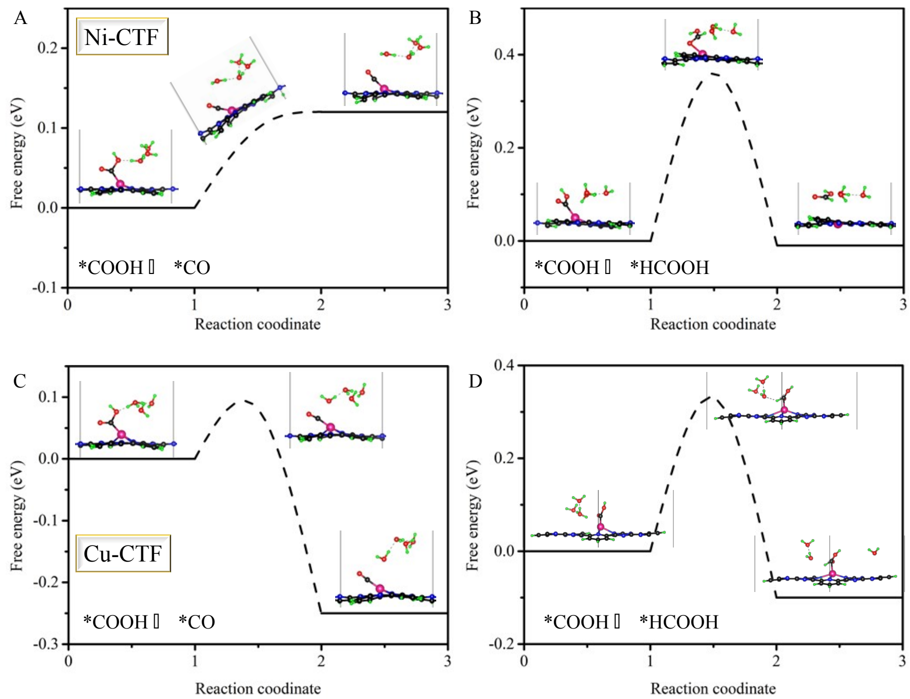

Figure S17. The transition state (TS) calculations of the elementary reactions toward *CO or *HCOOH intermediates on Ni-CTF (A, B) and Cu-CTF (C, D).

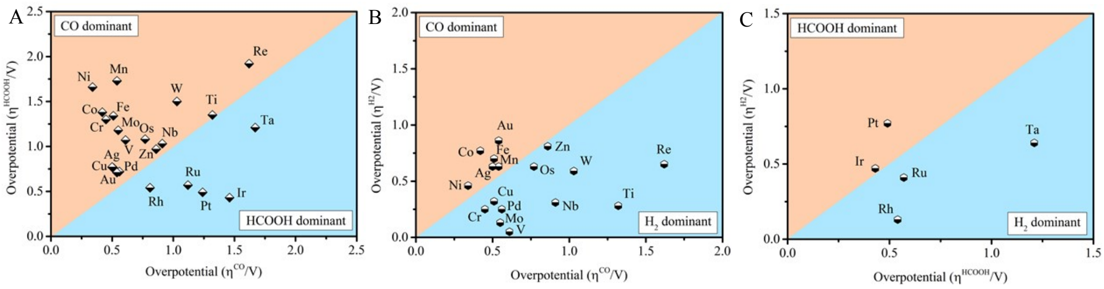

Figure S18. (A) The overpotential of CO (η^{CO}) as a function of the overpotential of HCOOH (η^{HCOOH}); (B) The overpotential of CO (η^{CO}) as a function of the overpotential of H_2 (η^{H2}); (C) The overpotential of HCOOH (η^{HCOOH}) as a function of the overpotential of H_2 (η^{H2}).

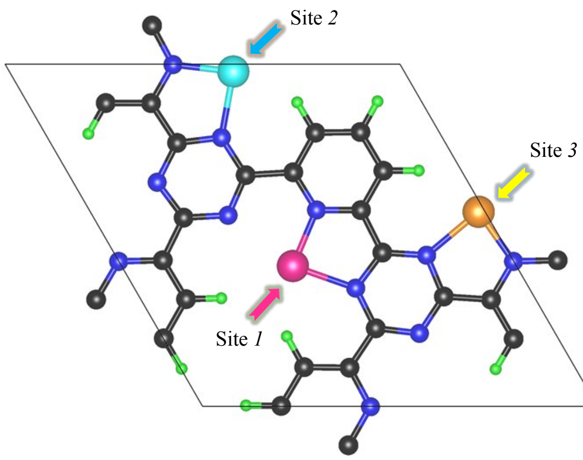

Figure S19. Three possible active sites in a unit, including site 1, site 2, site 3. The black, green, blue, red, pink, cyan and orange balls represent carbon hydrogen, nitrogen, oxygen, TM_1, TM_2, and TM_3 atoms, respectively. Note here, these three TM atoms can be homometallic or heterometallc.

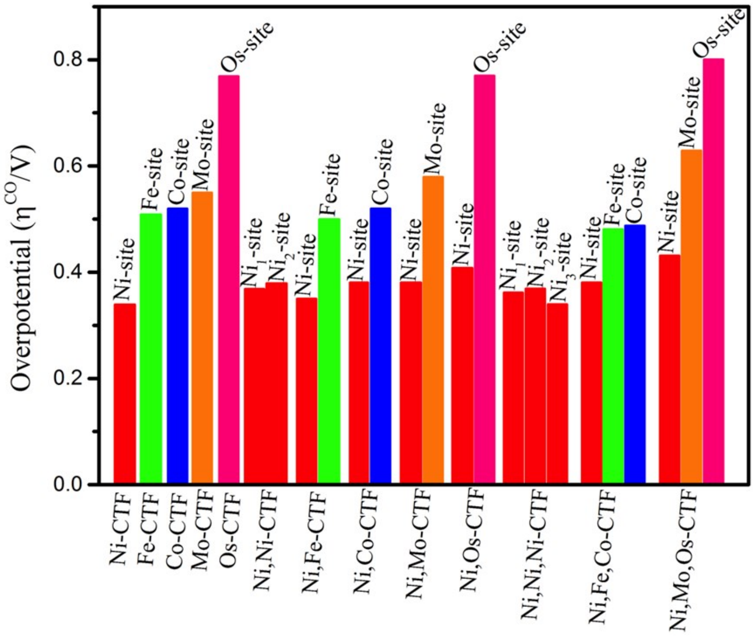

Figure S20. The catalytic activity (η^{CO}) in electrocatalytic CO_2 to CO on single, double, triple TM-CTFs.

References

[1]. Hansen, H. A.; Varley, J. B.; Peterson, A. A.; Nørskov, J. K. Understanding Trends in the Electrocatalytic Activity of Metals and Enzymes for CO_2 Reduction to CO. *J. Phys. Chem. Lett.* **2013**, *4*, 388–392.

[2]. Hirunsit, P. Electroreduction of carbon dioxide to methane on copper, copper–silver, and copper–gold catalysts: a DFT study. *J. Phys. Chem. C* **2013**, *117*, 8262–8268.

[3]. Karamad, M.; Hansen, H. A.; Rossmeisl, J.; Nørskov, J. K. Mechanistic Pathway in the Electrochemical Reduction of CO_2 on RuO_2. *ACS Catal.* **2015**, *5*, 4075–4081.

[4]. Peterson, A. A.; Abild-Pedersen, F.; Studt, F.; Rossmeisl, J.; Nørskov, J. K. How copper catalyzes the electroreduction of carbon dioxide into hydrocarbon fuels. *Energy Environ. Sci.* **2010**, *3*, 1311–1315.

[5]. Zhao, Z.; Lu, G. Computational Screening of Near-Surface Alloys for CO_2 Electroreduction. *ACS Catal.* **2018**, *8*, 3885–3894.

[6]. Chai, G.-L.; Guo, Z.-X. Highly effective sites and selectivity of nitrogen-doped

graphene/CNT catalysts for CO_2 electrochemical reduction. *Chem. Sci.* **2016**, *7*, 1268–1275.

[7]. Wu, J.; Yadav, R. M.; Liu, M.; Sharma, P. P.; Tiwary, C. S.; Ma, L.; Zou, X.; Zhou, X.-D.; Yakobson, B. I.; Lou, J.; Ajayan, P. M. Achieving Highly Efficient, Selective, and Stable CO_2 Reduction on Nitrogen-Doped Carbon Nanotubes. *ACS Nano* **2015**, *9*, 5364–5371.

[8]. Karamad, M.; Tripkovic, V.; Rossmeisl, J. Intermetallic Alloys as CO Electroreduction Catalysts-Role of Isolated Active Sites. *ACS Catal.* **2014**, *4*, 2268–2273.

[9]. Gong, L.; Zhang, D.; Lin, C.-Y.; Zhu, Y.; Shen, Y.; Zhang, J.; Han, X.; Zhang, L.; Xia, Z. Catalytic Mechanisms and Design Principles for Single-Atom Catalysts in Highly Efficient CO_2 Conversion. *Adv. Energy Mater.* **2019**, *9*, 1902625.

[10]. Ouyang, Y.; Shi, L.; Bai, X.; Li, Q.; Wang, J.; Breaking scaling relations for efficient CO_2 electrochemical reduction through dual-atom catalysts. *Chem. Sci.* **2020**, *11*, 1807-1813.

[11]. Henkelman, G.; Uberuaga, B. P.; Jónsson, H. A climbing image nudged elastic band method for finding saddle points and minimum energy paths. *J. Chem. Phys.* **2000**, *113*, 9901-9904.

[12]. Mathew, K.; Sundararaman, R.; Letchworth-Weaver, K.; Arias, T. A.; Hennig, R. G. Implicit solvation model for density-functional study of nanocrystal surfaces and reaction pathways. *J. Chem. Phys.* **2014**, 140, 084106.

[13]. Yuan, C.-Z.; Liang, K.; Xia, X.-M.; Yang, Z. K.; Jiang, Y.-F.; Zhao, T.; Lin, C.; Cheang, T.-Y.; Zhong, S.-L.; Xu, A.-W. Powerful CO_2 electroreduction performance with N–carbon doped with single Ni atoms. *Catal. Sci. Technol.* **2019**, *9*, 3669-3674.

[14]. Greeley, J.; Nørskov, J. K.; Electrochemical dissolution of surface alloys in acids: Thermodynamic trends from first-principles calculations. *Electrochim. Acta* **2007**, 52, 5829−5836.

[15]. Bard, A. J.; Parsons, R.; Jordan, J. Standard potentials in aqueous solution. Marcel Dekker, New York, **1985**.

[16]. M. J. Frisch, G. Trucks, H. B. Schlegel, G. Scuseria, M. Robb, J. Cheeseman, G. Scalmani, V. Barone, B. Mennucci and G. Petersson, Gaussian 09, Gaussian Inc., Wallingford CT, **2009**, 27, 34.

[17]. Becke, A. D. Density-functional thermochemistry. III. The role of exact exchange. *J. Chem. Phys.* **1993**, 98, 5648.

[18]. Solovyev, I. V.; Dederichs, P. H.; Anisimov, V. I. Corrected atomic limit in the local-density approximation and the electronic structure of d impurities in Rb. *Phys. Rev. B* **1994**, *50*, 16861–16871.

[19]. Anisimov, V. I.; Zaanen, J.; Andersen, O. K. Band theory and Mott insulators: Hubbard U instead of Stoner. *Phys. Rev. B* **1991**, *44*, 943.

[20]. Sekiyama, A.; Yamaguchi, J.; Higashiya, A.; Obara, M.; Sugiyama, H.; Kimura, M. Y.; Suga, S.; Imada, S.; Nekrasov, I. A.; Yabashi, M.; Tamasaku, K.; Ishikawa, T. The prominent 5d-orbital contribution to the conduction electrons in gold. *New J. Phys.* **2010**, *12*, 043045.

[21]. Himmetoglu, B.; Floris, A.; Gironcoli, S. d.; Cococcioni, M. Hubbard-corrected DFT energy functionals: The LDA+U description of correlated systems. *Int. J. Quantum Chem.* **2014**, *114*, 14–49.

[22]. Lin, C.-Y.; Zhang, L.; Zhao, Z.; Xia, Z. Design principles for covalent organic frameworks as efficient electrocatalysts in clean energy conversion and green oxidizer production. *Adv. Mater.* **2017**, *29*, 1606635.

[23]. Clementi, E.; Raimondi, D. L.; Reinhardt, W. P. Atomic screening constants from SCF functions. II. Atoms with 37 to 86 electrons. *J. Chem. Phys.* **1967**, *47*, 1300–1307.

[24]. Su, P.; Iwase, K.; Harada, T.; Kamiya, K.; Nakanishi, S. Covalent triazine framework modified with coordinatively-unsaturated Co or Ni atoms for CO_2 electrochemical reduction. *Chem. Sci.* **2018**, *9*, 3941–3947.

[25]. Wang, X.; Chen, Z.; Zhao, X.; Yao, T.; Chen, W.; You, R.; Zhao, C.; Wu, G.; Wang, J.; Huang, W.; Yang, J.; Hong, X.; Wei, S.; Wu, Y.; Li, Y. Regulation of Coordination Number over Single Co Sites: Triggering the Efficient Electroreduction of CO_2. *Angew. Chem. Int. Ed.* **2018**, *57*, 1944–1948.

[26]. Yan, C.; Li, H.; Ye, Y.; Wu, H.; Cai, F.; Si, R.; Xiao, J.; Miao, S.; Xie, S.; Yang, F.; Li, Y.; Wang, G.; Bao, X. Coordinatively unsaturated nickel–nitrogen sites towards selective and high-rate CO_2 electroreduction. *Energy Environ. Sci.* **2018**, *11*, 1204–1210.

[27]. Zheng, W.; Yang, J.; Chen, H.; Hou, Y.; Wang, Q.; Gu, M.; He, F.; Xia, Y.; Xia, Z.; Li, Z.; Yang, B.; Lei, L.; Yuan, C.; He, Q.; Qiu, M.; Feng, X. Atomically Defined Undercoordinated Active Sites for Highly Efficient CO_2 Electroreduction. *Adv. Funct. Mater.* **2020**, *30*, 1907658.

[28]. Rong, X.; Wang, H.-J.; Lu, X.-L.; Si, R.; Lu, T.-B. Controlled Synthesis of a Vacancy-Defect Single-Atom Catalyst for Boosting CO_2 Electroreduction. *Angew. Chem. Int. Ed.* **2020**, *59*, 1961–1965.

[29]. Wang, T.; Sang, X.; Zheng, W.; Yang, B.; Yao, S.; Lei, C.; Li, Z.; He, Q.; Lu, J.; Lei, L.; Dai, L.; Hou, Y. Gas Diffusion Strategy for Inserting Atomic Iron Sites into Graphitized Carbon Supports for Unusually High-Efficient CO_2 Electroreduction and High-Performance Zn–CO_2 Batteries. *Adv. Mater.* **2020**, *32*, 2002430.

[30]. Su, P.; Iwase, K.; Nakanishi, S.; Hashimoto, K.; Kamiya, K. Nickel-nitrogen-modified graphene: an efficient electrocatalyst for the reduction of carbon dioxide to carbon monoxide. *Small* **2016**, *12*, 6083–6089.

[31]. Daiyan, R.; Zhu, X.; Tong, Z.; Gong, L.; Razmjou, A.; Liu, R.-S.; Xia, Z.; Lu, X.; Dai, L.; Amal, R. Transforming active sites in nickel–nitrogen–carbon catalysts for efficient electrochemical CO_2 reduction to CO. *Nano Energy* **2020**, *78*, 105213.